Plasma propagation of a 13.56 MHz asymmetric surface barrier discharge in atmospheric pressure air

2011 J. Phys. D: Appl. Phys. 44 205202

(http://iopscience.iop.org/0022-3727/44/20/205202)

J. Phys. D: Appl. Phys. **44** (2011) 205202 (8pp) doi:10.1088/0022-3727/44/20/205202

Plasma propagation of a 13.56 MHz asymmetric surface barrier discharge in atmospheric pressure air

J Dedrick[1], R W Boswell[1], P Audier[2], H Rabat[2], D Hong[2] and C Charles[1]

[1] Space Plasma, Power and Propulsion Group, Research School of Physics and Engineering, The Australian National University, ACT 0200, Australia
[2] GREMI - UMR6606 CNRS/Université d'Orléans, Polytech'Orléans, 14, rue d'Issoudun - BP6744, 45067 ORLEANS Cedex 2, France

E-mail: james.dedrick@anu.edu.au

Received 20 January 2011, in final form 29 March 2011
Published 3 May 2011
Online at stacks.iop.org/JPhysD/44/205202

Abstract
The propagation of an rf asymmetric surface barrier discharge in atmospheric pressure air has been investigated. Measurements of the pulse-modulated 13.56 MHz voltage and current together with ICCD images of the plasma were recorded to study the visible plasma structure with respect to the rf pulses, time within the pulses and the rf waveforms. When exposing images over full rf pulses, which comprise over 150 oscillations of the applied voltage, clearly defined filamentary structures are observed indicating a strong memory effect. The discharge intensity decreases exponentially with distance from the electrode edge, and the average propagation length increases linearly with the applied voltage. Similar to some lower frequency asymmetric surface dielectric barrier discharges, two distinct breakdown events occur during one period of the voltage waveform. The number of filaments is found to be the same for both breakdown events, and collective effects are observed in both discharges.

(Some figures in this article are in colour only in the electronic version)

1. Introduction

Non-thermal plasma discharges operating at atmospheric pressure have applications in many areas, including industrial processing [1], materials science [2] and aerodynamics [3]. Although a wide range of configurations can be used, variations of the dielectric barrier discharge (DBD) [4], atmospheric pressure plasma jet (APPJ) [5], dc corona discharge [6], cold plasma torch [7], coplanar surface discharge [8] and inductively coupled reactor [9] are typically used.

A configuration known as an asymmetric surface dielectric barrier discharge (ASDBD) has received significant interest due to its capability to promote aerodynamic flow control [10–12]. Although DBDs may be driven over a wide range of frequencies up to 500 kHz [13], they have been found to perform most effectively at up to about 10 kHz and recently with ns pulses [14] using applied voltages of several kV. Experimental [15–19], modelling [20, 21] and simulation studies [22] have been undertaken in order to understand the underlying physics of these aerodynamic actuators and to optimize their performance.

For atmospheric pressure air plasmas, the discharge volume is typically too small to allow direct diagnostic access. However, their properties may still be investigated remotely. For example, fast imaging has been used to analyse the spatio-temporal discharge characteristics in the glow [23–27] and non-diffuse modes [28, 29]. These studies build upon research utilizing Pockels effect [30] and dust figures [31] to investigate the factors influencing the structure of the discharge [32]. Time-resolved spectroscopy has also been used to identify the behaviour of specific excited species within the plasma [33].

The spatio-temporal structure of streamers in ASDBDs has previously been investigated [34–37]. These studies found that two distinct intervals of plasma activation occur during the times when the slew rate of the voltage is at a maximum, i.e. at the zero crossings, and that each discharge terminates

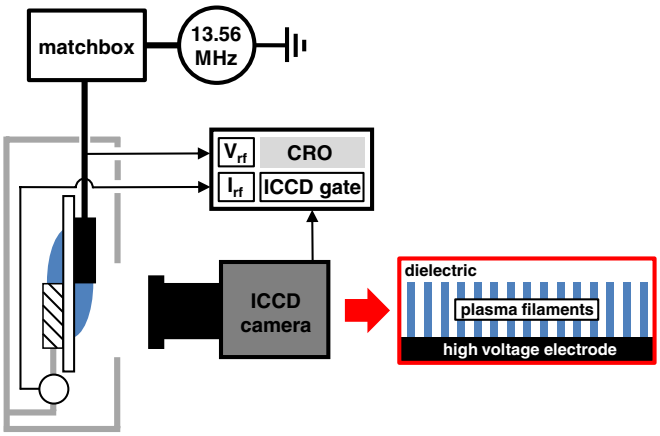

Figure 1. Schematic of the reactor showing a surface plasma on both sides of the dielectric (white), the electrical probes and the image acquisition system. The hv and grounded electrodes are depicted in black and hatching, respectively. A cartoon of the discharge, as imaged by the camera, is shown right.

at the maxima/minima of the voltage waveform when the displacement current in the gap approaches zero.

In capacitively coupled discharges driven at several MHz, breakdown can be dominated by electron diffusion if the amplitude of oscillation is small compared with the electrode spacing [38]. This may increase the stability of the discharge compared with DBDs if the voltage required to activate the plasma is reduced [39]. Such high frequency, low voltage surface discharges could potentially provide localized, fast heating to aerodynamic boundary layers, which has been shown to be an effective flow control technique [14, 40]. In this study, we use fast imaging to study the propagation and plasma structure of a 13.56 MHz asymmetric surface barrier discharge in atmospheric pressure air for comparison with ASDBDs currently under development as aerodynamic actuators.

2. Experiment details

2.1. Reactor configuration

The experiment reactor is shown in figure 1 and has previously been described in further detail [41]. Two identical electrodes are wire-cut from 0.25 mm thick copper sheet to a width of 10 mm and each corner is radiused to 1 mm to minimize edge effects. These electrodes are held by clamps on either side of a 0.2 mm thick, opaque dielectric layer of mica (capacitance 50 pF). The active electrode length for the discharge is 40 mm, and the plasma activates on both sides of the dielectric barrier. In this investigation, only the plasma propagating from the powered, high voltage (hv) electrode is imaged and the discharge on the other side of the dielectric barrier is not visible. The experiments are conducted in the ambient air of the laboratory which is approximately at atmospheric pressure.

A 75 MHz hv probe is used to measure the voltage applied to the powered electrode and the return current is determined using a 50 MHz Rogowski coil fitted between the electrode on the other side of the dielectric and its grounding point. An *Andor iStar* ICCD camera (1024 × 1024, 13 μm^2 pixels) with a 35–105 mm lense is installed 250 mm in front of the breakdown region and is protected from rf radiation as much as possible using a wire mesh screen. The electrical probes are connected to a 600 MHz *LeCroy WaveSurfer* oscilloscope with a sampling speed of 2.5 GHz.

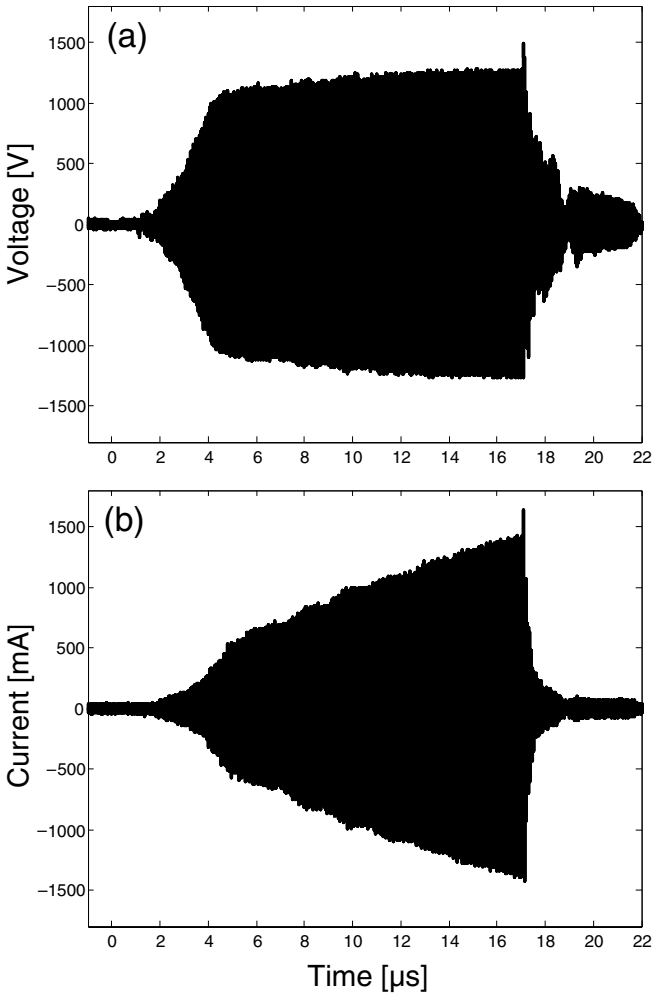

Figure 2. (*a*) rf voltage and (*b*) current pulses for $P_{real} = 450$ W.

2.2. Electrical measurements

Rf power at 13.56 MHz is applied to the hv electrode with a pulse modulation of 10 kHz and a duty cycle of 15%, which corresponds to a total pulse duration of about 15 μs. A duty cycle of 15% is the smallest possible when pulsing this generator at 10 kHz. This was chosen to minimize dielectric heating, while keeping the pulse frequency consistent with previous work. Adequate power coupling is achieved using a matching network with variable capacitors. The power P_{real} input to the matching network is measured by the generator, and is equal to the forward power minus the reflected power.

The rf voltage and current pulses for $P_{real} = 450$ W are shown in figure 2. Both the voltage (figure 2(*a*)) and current (figure 2(*b*)) exhibit distinct bumps approximately 4.5 μs into the pulse when the plasma breaks down. Subsequently, the amplitude of the voltage remains relatively constant until the termination point at 17 μs while the amplitude of the current increases steadily. This indicates that the frequency of the

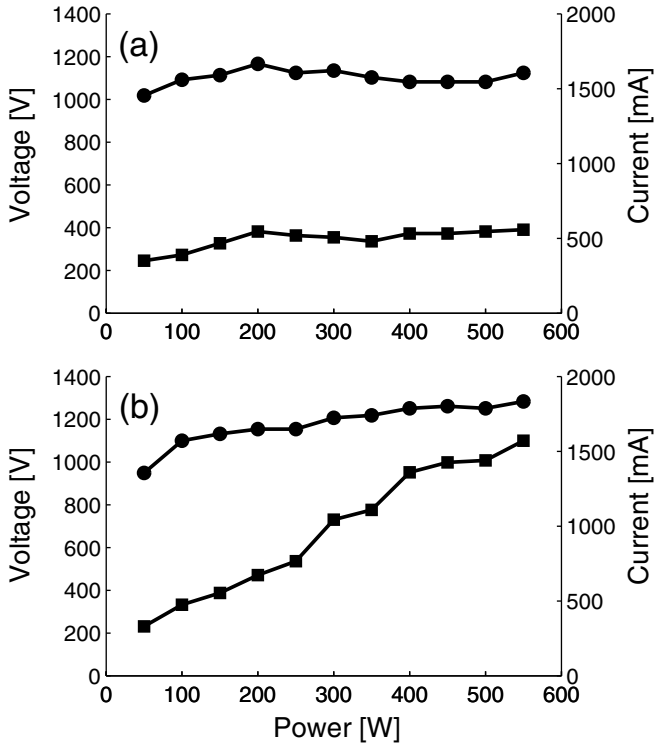

Figure 3. Amplitude of (*a*) the voltage (circles) and current (squares) at the breakdown point 4.5 μs into the pulse and (*b*) at the termination point.

applied voltage is sufficient to promote an increase in the presence of free charges over successive rf periods, but these are then lost before the beginning of the next pulse.

When P_{real} is increased through 50–550 W, the amplitude of the pulse dilates, i.e. the shape of the pulse envelope does not remain constant. As shown in figure 3, the amplitudes of the voltage and current at the moment of breakdown (figure 3(*a*)) remain relatively steady for increasing power. The amplitude of the current increases by a factor of 5 when measured at the end of the pulse (figure 3(*b*)) while the increase in the voltage remains relatively small. Small increases in the voltage applied to the reactor lead to larger increases in the measured current at the termination point of the pulse.

2.3. Image acquisition

The oscilloscope is set to trigger an image acquisition when the voltage applied to the hv electrode reaches approximately 300 V at the beginning of an rf pulse (at approximately 3 μs in figure 2). This trigger is amplified with a pulse generator and sent to the ICCD to start an exposure sequence with a delay due to the electronics of approximately 80 ns. An additional delay time between the moment when the ICCD intensifier activates and the beginning of the exposure, and the exposure time itself, are controlled via a computer and displayed on the oscilloscope as a combined pulse. Three different exposure times, 2 ns, 74 ns or 20 μs, were used to study the propagation over different time intervals as detailed in the results section. For a chosen exposure time, the intensifier delay can be adjusted so that the acquisition correlates with the region of interest with respect to the voltage and current waveforms.

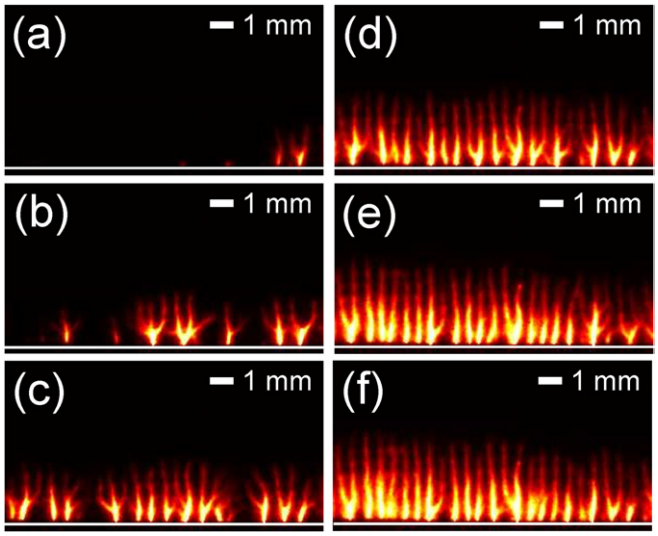

Figure 4. Images of the plasma for (*a*)–(*f*) P_{real} of 100 W, 200 W, 300 W, 400 W, 500 W and 550 W, respectively. The white lines indicate the location of the hv electrode edge.

Each image usually requires a couple of seconds to be triggered, acquired and recorded and so sequential time intervals are imaged over several pulses. In all cases, the images are recorded as single shots to maximize the clarity of the discharges. Each image is normalized with respect to the mean grey value of its bottom-half (where no plasma is active) and the length scale is calibrated by imaging mm paper alongside the hv electrode.

3. Results: time-resolved ICCD imaging

3.1. Imaging over the entire pulse

(i) *Macroscopic structure.* Images of the plasma gated over the full rf pulse (20 μs exposure time) for $P_{\text{real}} = 100$–550 W are shown in figure 4. Even though the camera is gated over approximately 170 rf cycles (between the breakdown and termination points), clearly defined discharges propagate approximately 2.5 mm away from the edge of the hv electrode over the surface of the dielectric, which prevents direct contact between the plasma and the grounded electrode underneath (see figure 1). This indicates that their propagation is not random, and that they form in relatively fixed locations probably due to the memory effect. At lower powers (figures 4(*a*)–(*c*)), the discharges are not spaced regularly and a high degree of branching if observed. As the applied power is increased further (figures 4(*d*)–(*f*)), the distribution becomes more uniform as the plasma channels extend further over the surface in single or double branches.

The properties of the dielectric layer are important in determining the degree of charge accumulation, electron trapping the distribution of the electric field. The deformations present on the mica surface were measured with a profilometer and are spaced every 500 μm (measured as the average distance between to adjacent peaks) with a mean height deviation

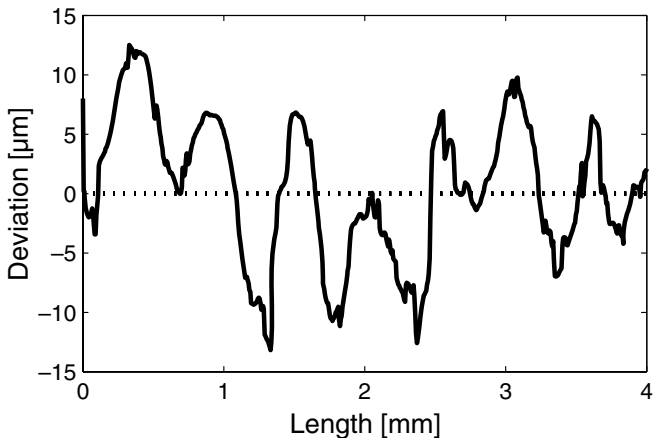

Figure 5. Surface profile of the mica dielectric barrier imaged by the camera.

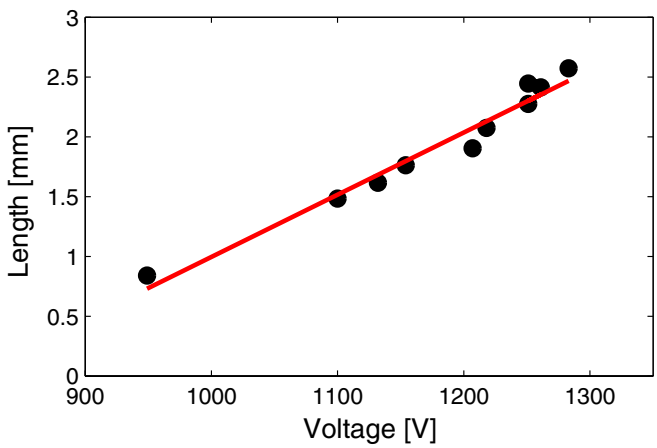

Figure 6. Mean propagation length of the plasma with respect to the amplitude of the voltage at the termination point of the pulse.

of 3 μm as shown in figure 5. The spacing between these depressions is quite similar to that between the tips of the filaments shown in figures 4(*d*)–(*f*), suggesting that the roughness of the dielectric may influence the spacing of the filaments. The structure of the discharges is not observed to change significantly for different orientations of the dielectric.

(ii) *Propagation length and voltage.* Many previous studies have found a linear correlation between the maximum plasma extension and the applied voltage, for example [36, 37]. Here, we define the edge of the filaments as the length at which the intensity, averaged across the electrode span, drops to 5% of its maximum value. As shown in figure 6, when the voltage at the termination point of the pulse is used, i.e. when the current is at a maximum, we also find a linear relationship between it and the average propagation length. As discussed later, a similar result is observed with respect to the applied voltage waveform.

(iii) *Intensity distribution with respect to propagation length.* The images in figure 4 show that the discharge intensity is not constant with respect to the perpendicular distance away from the electrode edge. Previous work by Orlov using a photomultiplier tube to measure the optical emission from a plasma actuator driven at 5 kV and 5 kHz found that the

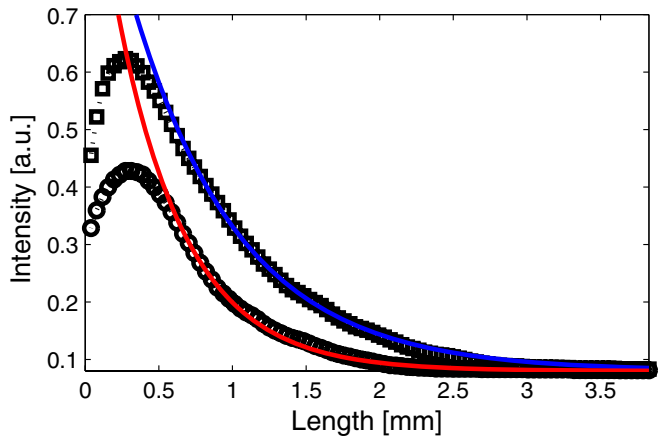

Figure 7. Mean intensity of the plasma with respect to the perpendicular distance away from the hv electrode. The two cases of $P_{\text{real}} = 300$ W (circles) and 500 W (squares) can be fitted with decaying exponential functions.

intensity of the discharge could be fitted to an exponential decaying function of the form $y = \mathrm{e}^{-x/a}$ where x is the average extension length and a is the rate of decay [35]. Others have proposed a half-Gaussian fit for the use in numerical modelling of the force generation by plasma actuators [42]. The optical emission intensity is proportional to the electron density multiplied by a function of the electron temperature (or the electron velocity distribution function). Hence for a constant electron temperature it is reasonable to propose that the electron density would be proportional to the optical emission intensity suggesting that the electron density also decreases exponentially away from the electrode edge.

The average intensity of this discharge was investigated with respect to the perpendicular distance away from the hv electrode for two input power cases of $P_{\text{real}} = 300$ W and 500 W. As shown in figure 7, beyond an extension length of 0.6 mm from the hv electrode edge, these distributions can be fitted with an exponential function of the same form with the coefficient a equalling 0.47 and 0.725, respectively.

3.2. *Imaging throughout the rf pulses*

As shown in figure 2, the degree of power coupling into the discharge is not steady during the rf pulses. To determine the changes in plasma properties throughout the voltage and current pulses, images were exposed over one rf period (74 ns at 13.56 MHz) at 1 μs intervals. This interval size was decreased to 0.25 μs during the breakdown and termination of the discharge at the beginning and end of the pulse, respectively.

Figure 8 shows the normalized voltage and current pulses for $P_{\text{real}} = 450$ W (see figure 2) when they are overlaid with the number and mean intensity of the discharges propagating from the hv electrode (also normalized). We observe that the discharge initiates at approximately 1.1 kV as shown by the sharp increase in the average intensity 4.5 μs into the pulse. It is also possible to obtain small, randomly spaced filaments for applied voltages as low as 950 V.

The profile of the current pulse (figure 8(*a*)) correlates closely with the mean intensity, while the profile of the

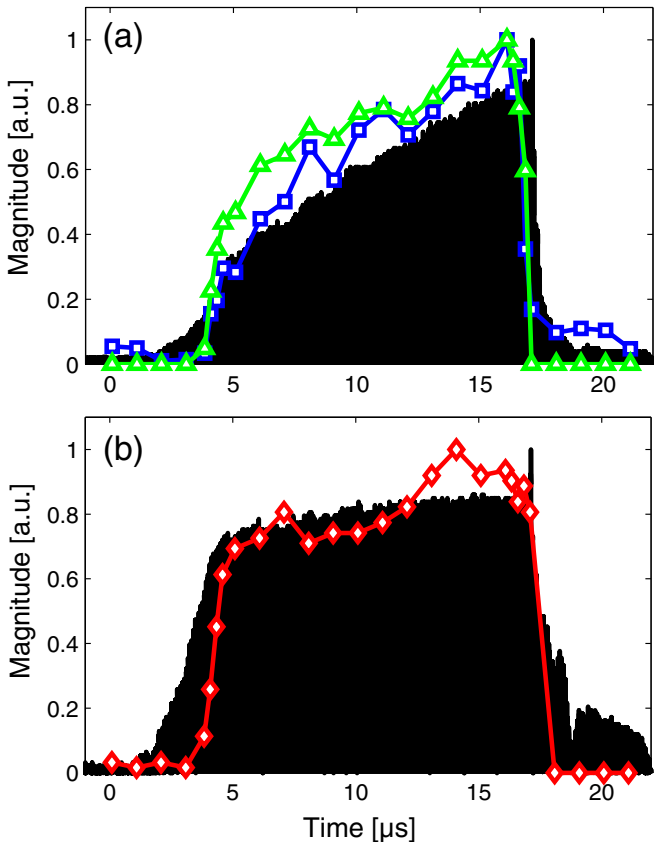

Figure 8. Normalised measurements of the (*a*) current (black), intensity (squares) and number of discharge tips (triangles) together with (*b*) voltage (black) and number of discharge stems (diamonds) throughout the pulse for $P_{\mathrm{real}} = 450$ W.

voltage pulse (figure 8(*b*)) agrees more closely with the number of initiating discharges. This may appear to disagree with previous findings [36], but may be explained by considering the degree of branching. When the number of discharges at the maximum extension length from the hv electrode, i.e. tips, are compared with that close to the electrode edge, i.e. stems, we find that the increasing current may be accommodated through branching rather than the initiation of new filaments. These measurements were undertaken for two additional input powers of 200 and 300 W with the same result.

3.3. Imaging throughout the voltage waveform

The propagation relative to the applied voltage waveform V_{rf} was studied by exposing the ICCD over successive 2 ns intervals. A single-period interval towards the end of the rf pulses was chosen since this is when the optical emission from the plasma is most intense. It was important to ensure that successive exposures did not overlap in time, as this would result in an incorrect calculation for the mean intensity of the image. In order to resolve each interval precisely, the acquisitions were triggered from the ICCD controller by adding 2 ns to the delay each time. The capability of this method was then confirmed by comparing these images with those acquired by triggering the acquisition manually with the oscilloscope.

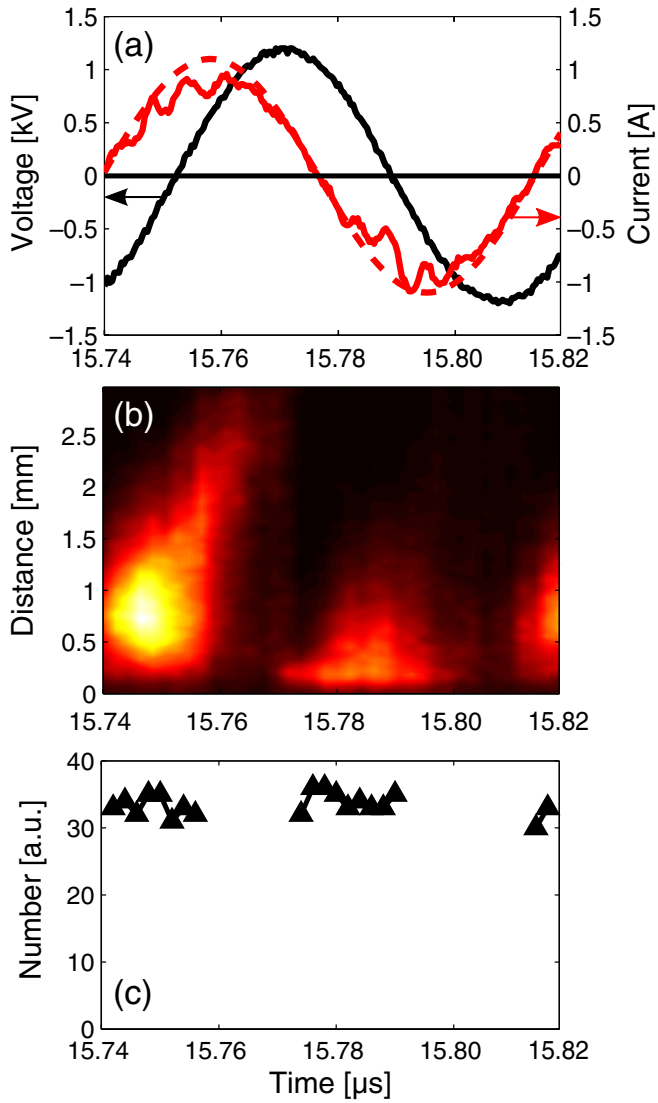

Figure 9. (*a*) Variation of the applied voltage (black) and return current (red with a dashed sinusoidal fit) nearby to the termination point of a pulse for $P_{\mathrm{real}} = 450$ W, (*b*) temporal distribution of intensity with respect to perpendicular distance away from the electrode and (*c*) number of filaments measured at the hv electrode edge.

The applied voltage V_{rf} and return current are shown in figure 9(*a*) for one rf period towards the termination point of a pulse for $P_{\mathrm{real}} = 435$ W. The waveforms are those for the first image, although very little variation was observed in subsequent acquisitions. A sinusoidal current trace, for which the zero crossing and gradient at the zero crossing match those of the measurement, has also been included. The voltage waveform is almost completely sinusoidal. Before and after plasma activation the current is sinusoidal and leads the voltage by a quarter of an rf period as is expected for a capacitively coupled system. When the plasma breaks down, the increased inductance of the discharge region causes the phase difference to decrease. There are clear variations in the current trace away from a sinusoidal waveform as observed in other rf capacitively coupled discharge systems [39]. These occur during both the rising and falling portions of V_{rf} and increase in magnitude throughout the rf pulse.

The corresponding emission intensity is shown in figure 9(*b*). When the plasma is active, discharges of similar dimension and intensity appear equally spaced along the electrode span. At each time-step, the intensity is averaged across the electrode length and plotted with respect to the perpendicular distance away from the electrode. In agreement with previous studies [35–37], we observe that the optical emission is dependent upon V_{rf}. Two distinct breakdown events are evident within one rf period and this pattern continues into the next cycle.

The number of discharges present during each 2 ns acquisition interval was counted by measuring the intensity of the image across a row of pixels close to the hv electrode (figure 9(*c*)). We only count the number of discharges initiating from the hv electrode and do not consider the effects of branching. Using this method, the number of filaments is observed to be the same for both types of discharge.

Since the moments when the current waveform deviate from a sinusoid correspond to moments of discharge activity, and the number of discharges propagating from the hv electrode remains relatively constant throughout the discharge, we can estimate the average charge transfer per microdischarge using

$$Q = \frac{1}{N} \int \Delta i \, \mathrm{d}t, \qquad (1)$$

where N is the average number of microdischarges (see figure 9(*c*)) and Δi is the absolute difference between the measured current and the fitted sinusoid during the times when optical emission from the plasma is recorded (see figure 9(*b*)). For the positive-going discharge, we get 0.13 nC of charge transfer per streamer and 0.12 nC in the negative-going case. These values are within the range of those previously observed for single microdischarges in air and are not considered to be pressure dependent [4].

It is important to note that the measured current comprises parts from both the imaged discharge and that on the opposite side of the dielectric (not visible). The latter discharge was also imaged and showed almost identical behaviour to the former, although was one half-period out of phase. Therefore, the mean charge transfer per streamer calculated above is the sum of the higher intensity discharge from one side of the dielectric and the lower-intensity discharge from the other side. This explains why both perturbation intervals correspond to a comparable transfer of charge.

The longer, more intense plasma is observed to occur when V_{rf} has just passed a local minimum and is rising past the positive-going zero crossing. The plasma appears as elongated filaments which have also been observed in the same portion of the applied voltage for lower frequency ASDBDs [36, 37]. A second breakdown event, for which the discharges propagate only one third the distance of the first, occurs during the negative-going portion of V_{rf}. For both discharge events, the filaments increase in length as a linear relation to the applied voltage, and the propagation velocity is determined to be 6.9×10^4 m s^{-1} and 3.7×10^4 m s^{-1}, respectively. These values are the same order of magnitude as those measured by Hoskinson *et al* for an ASDBD driven by a 7 kV and 1 kHz triangular waveform [37].

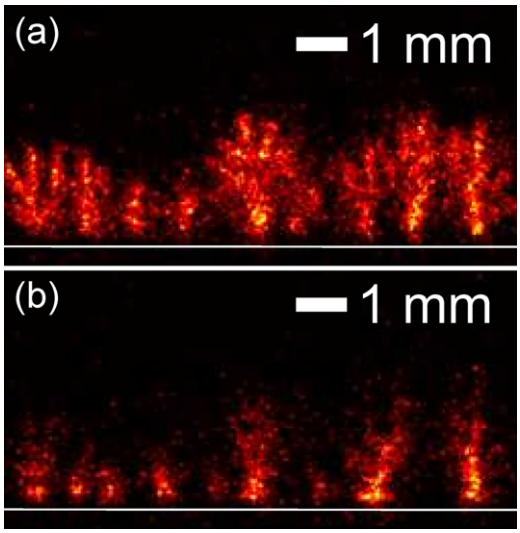

Figure 10. Images of the plasmas at their point of greatest intensity during (*a*) the positive-going and (*b*) negative-going activations. The white lines indicate the location of the hv electrode edge.

When V_{rf} approaches a maximum or minimum value, i.e. when the displacement current in the discharge region approaches zero, both discharges rapidly terminate, although the speed at which they retract is different. For the larger discharge, the retraction takes only a few ns while the smaller, less intense breakdown takes approximately 10 ns to decay on average.

The visible appearance of the two discharges at their maximum intensities are shown in figure 10. When V_{rf} is rising (figure 10(*a*)), the larger-intensity discharge occurs and the filaments are longer and more slender, while in the lower-intensity activation they are shorter, broader and more diffuse (figure 10(*b*)).

The synchronized breakdown of plasma channels from a single current peak, known commonly as the collective effect, has previously been studied for atmospheric pressure discharges. During the positive-going phase of the voltage, this is thought to be caused by the emission of photons from the initiating streamer since they are the only species capable of diffusing fast enough [43]. The collective effect is considered less likely during the negative-going phase, and previous work by Allegraud *et al* found that in this case single current peaks result in single streamers for an ASDBD at 50 Hz [36]. At 13.56 MHz, the observation of collective effects for both rising and falling voltages, and the similarity in the current trace perturbations over both intervals, suggests that the significantly faster rise time of the voltage may play a greater role here.

Although the discharge studied here shares some similar characteristics to that of ASDBD plasma actuators, the increased voltage slew rate and decreased voltage amplitude are expected to influence the interaction between the plasma particles and the neutral gas. Further investigation is therefore required to directly measure the capability of the rf driven surface plasma to act as an aerodynamic actuator.

4. Conclusion

The propagation of an rf asymmetric surface barrier discharge in atmospheric pressure air has been investigated experimentally. The results can be summarized as follows:

- The voltage oscillations are of sufficient frequency to trap electrons in the discharge region across successive rf cycles, and this leads to an increase in the length, intensity and degree of branching of the discharge throughout the pulse. The rapid oscillations of the driving voltage may also be responsible for the stationary appearance of the filaments due to a local reduction in the breakdown field remaining from previous activations.
- The mean propagation length has been studied with respect to the applied voltage pulses and waveforms, and varies linearly with the applied voltage in both cases.
- The distribution of intensity varies exponentially with perpendicular distance away from the hv electrode, and this trend begins 0.6 mm from the electrode edge.
- We have observed the collective breakdown of filaments across the full electrode length for both the positive-going and negative-going portions of the applied voltage.

Acknowledgments

The authors wish to thank the Australian French Association for Science and Technology ACT (AFAS, ACT) for their financial support for overseas travel. The technical assistance of P Alexander, P Brault and A Caillard is also most appreciated.

References

[1] Kogelschatz U 2004 Atmospheric-pressure plasma technology *Plasma Phys. Control. Fusion* **46** B63–B75
[2] Wagner H E, Brandenburg R, Kozlov K V, Sonnenfeld A, Michel P and Behnke J F 2003 The barrier discharge: basic properties and applications to surface treatment *Vacuum* **71** 417–36
[3] Braun E M, Lu F K and Wilson D R 2009 Experimental research in aerodynamic control with electric and electromagnetic fields *Prog. Aerospace Sci.* **45** 30–49
[4] Kogelschatz U, Eliasson B and Egli W 1997 Dielectric-barrier discharges. Principle and applications *J. Phys. IV* **7** 47–66
[5] Schütze A, Jeong J Y, Babayan S E, Park J, Selwyn G S and Hicks R F 1998 The atmospheric-pressure plasma jet: a review and comparison to other plasma sources *IEEE Trans. Plasma Sci.* **26** 1685–94
[6] Antao D S, Staack D A, Fridman A and Farouk B 2009 Atmospheric pressure dc corona discharges: operating regimes and potential applications *Plasma Sources Sci. Technol.* **18** 035016
[7] Koinuma H, Ohkubo H, Hashimoto T, Inomata K, Shiraishi T, Miyanaga A and Hayashi S 1992 Development and application of a microbeam plasma generator *Appl. Phys. Lett.* **60** 816–17
[8] Šimor M, Ráhel' J, Vojtek P and Černák M 2002 Atmospheric-pressure diffuse coplanar surface discharge for surface treatments *Appl. Phys. Lett.* **81** 2716–18
[9] Hopwood J A 2000 A microfabricated inductively coupled plasma generator *J. Microelectromech. Syst.* **9** 309–13
[10] Roth J R 2003 Aerodynamic flow acceleration using paraelectric and peristaltic electrohydrodynamic effects of a one atmosphere uniform glow discharge plasma *Phys. Plasmas* **10** 2117–26
[11] Corke T C, Enloe C L and Wilkinson S P 2010 Dielectric barrier discharge plasma actuators for flow control *Annu. Rev. Fluid Mech.* **42** 505–29
[12] Moreau E 2007 Airflow control by non-thermal plasma actuators *J. Phys. D: Appl. Phys.* **40** 605–36
[13] Fridman A, Chirokov A and Gutsol A 2005 Non-thermal atmospheric pressure discharges *J. Phys. D: Appl. Phys.* **38** R1–R24
[14] Starikovskii A Y, Nikipelov A A, Nudnova M M and Roupassov D V 2009 SDBD plasma actuator with nanosecond pulse-periodic discharge *Plasma Sources Sci. Technol.* **18** 034015
[15] Balcon N, Benard N, Lagmich Y, Bouef J P, Touchard G and Moreau E 2009 Positive and negative sawtooth signals applied to a DBD plasma actuator—influence on the electric wind *J. Electrostatics* **67** 140–45
[16] Forte M, Jolibois J, Pons J, Moreau E, Touchard G and Cazalens M 2007 Optimization of a dielectric barrier discharge actuator by stationary and non-stationary measurements of the induced flow velocity: application to airflow control *Exp. Fluids* **43** 917–28
[17] Hoskinson A R and Hershkowitz N 2010 Differences between dielectric barrier discharge plasma actuators with cylindrical and rectangular exposed electrodes *J. Phys. D: Appl. Phys.* **43** 065205
[18] Kim W, Do H, Mungal M G and Cappelli M A 2007 On the role of oxygen in dielectric barrier discharge actuation of aerodynamic flows *Appl. Phys. Lett.* **91** 181501
[19] Dong B, Bauchire J M, Pouvesle J M, Magnier P and Hong D 2008 Experimental study of a DBD surface discharge for the active control of subsonic airflow *J. Phys. D: Appl. Phys.* **41** 155201
[20] Boeuf J P, Lagmich Y and Pitchford L C 2009 Contribution of positive and negative ions to the electrohydrodynamic force in a dielectric barrier discharge plasma actuator operating in air *J. Appl. Phys.* **106** 023115
[21] Jayaraman B and Shyy W 2008 Modeling of dielectric barrier discharge-induced fluid dynamics and heat transfer *Prog. Aerospace Sci.* **44** 139–91
[22] Singh K P and Roy S 2008 Physics of plasma actuator operating in atmospheric air *Appl. Phys. Lett.* **92** 111502
[23] Starostin S A, Antony Premkumar P, Creatore M, van Veldhuizen E M, de Vries H, Paffen R M J and van de Sanden M C M 2009 On the formation mechanisms of the diffuse atmospheric pressure dielectric barrier discharge in CVD processes of thin silica-like films *Plasma Sources Sci. Technol.* **18** 045021
[24] Shi J, Cai Y, Zhang J, Ding K and Zhang J 2009 Discharge ignition characteristics of pulsed radio-frequency glow discharges in atmospheric helium *Phys. Plasmas* **16** 070702
[25] Liu D W, Shi J J and Kong M G 2007 Electron trapping in radio-frequency atmospheric-pressure glow discharges *Appl. Phys. Lett.* **90** 041502
[26] Gherardi N, Gouda G, Gat E, Ricard A and Massines F 2000 Transition from glow silent discharge to micro-discharges in nitrogen gas *Plasma Sources Sci. Technol.* **9** 340–46
[27] Lu X and Laroussi M 2003 Ignition phase and steady-state structures of a non-thermal air plasma *J. Phys. D: Appl. Phys.* **36** 661–65
[28] Celestin S, Canes-Boussard G, Guaitella O, Bourdon A and Rousseau A 2008 Influence of the charges deposition on the spatio-temporal self-organization of streamers in a DBD *J. Phys. D: Appl. Phys.* **41** 205214

[29] van Veldhuizen E M and Rutgers W R 2002 Pulsed positive corona streamer propagation and branching *J. Phys. D: Appl. Phys.* **35** 2169–79
[30] Zhu Y, Takada T, Sakai K and Tux D 1996 The dynamic measurement of surface charge distribution deposited from partial discharge in air by Pockels effect technique *J. Phys. D: Appl. Phys.* **29** 2892–900
[31] Murooka Y, Takada T and Hidaka K 2001 Nanosecond surface discharge and charge density evaluation: I. Review and experiments *IEEE Electr. Insul.* **17** 6–16
[32] Chiba M, Kumada A and Hidaka K 2002 *IEEE Trans. Dielectr. Electr. Insul.* **9** 118–23
[33] Kozlov K V, Wagner H E, Brandenburg R and Michel P 2001 Spatio-temporally resolved spectroscopic diagnostics of the barrier discharge in air at atmospheric pressure *J. Phys. D: Appl. Phys.* **34** 3164–76
[34] Sasoh A, Kikuchi K and Sakai T 2007 Spatio-temporal filament behaviour in a dielectric barrier discharge plasma actuator *J. Phys. D: Appl. Phys.* **40** 4181–4
[35] Orlov D M 2006 Modelling and simulation of single dielectric barrier discharge plasma actuators *PhD Thesis* University of Notre Dame
[36] Allegraud K, Guaitella O and Rousseau A 2007 Spatio-temporal breakdown in surface DBDs: evidence of collective effect *J. Phys. D: Appl. Phys.* **40** 7698–706
[37] Hoskinson A R, Oksuz L and Hershkowitz N 2008 Microdischarge propagation and expansion in a surface dielectric barrier discharge *Appl. Phys. Lett.* **93** 221501
[38] Smith H, Charles C and Boswell R W 2003 Breakdown behavior in radio-frequency argon discharges *Phys. Plasmas* **10** 875–81
[39] Park J, Henins I, Herrmann H W and Selwyn G S 2001 Gas breakdown in an atmospheric pressure radio-frequency capacitive plasma source *J. Appl. Phys.* **89** 15–19
[40] Bletzinger P, Ganguly B N, Van Wie D and Garscadden A 2005 Plasmas in high speed aerodynamics *J. Phys. D: Appl. Phys.* **38** R33–R57
[41] Dedrick J, Boswell R W and Charles C 2010 Asymmetric surface barrier discharge plasma driven by pulsed 13.56 MHz power in atmospheric pressure air *J. Phys. D: Appl. Phys.* **43** 342001
[42] Suzen Y B, Huang P G, Jacob J D and Ashpis D E 2005 Numerical Simulations of plasma based flow control applications *35th Fluid Dynamics Conf. and Exhibit (Toronto, ON, June 2005) AIAA Paper* 2005-4633
[43] Guaitella O, Thevenet F, Guillard C and Rousseau A 2006 Dynamic of the plasma current amplitude in a barrier discharge: influence of photocatalytic material *J. Phys. D: Appl. Phys.* **39** 2964–72